

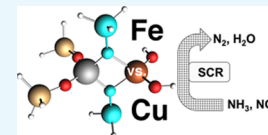
Computational Insights into the Mechanism of the Selective Catalytic Reduction of NO_x: Fe- versus Cu-Exchanged Zeolite Catalysts

Julian Rudolph and Christoph R. Jacob*[✉]

Institute of Physical and Theoretical Chemistry, Technische Universität Braunschweig, Gaußstraße 17, 38106 Braunschweig, Germany

Supporting Information

ABSTRACT: We computationally investigate the mechanism of the reduction half-cycle of the selective catalytic reduction of nitrogen oxides with ammonia. We compare both Fe- and Cu-exchanged zeolite catalysts and aim at exploring all accessible reaction pathways. From our calculations, a comprehensive picture emerges that unifies several previous mechanistic proposals. We find that both for Fe and for Cu catalysts different reaction pathways are feasible but some of the possible reaction pathways differ in these two cases. Our computational results provide a basis for the interpretation of in situ spectroscopic investigations that can possibly distinguish the different mechanistic pathways.



1. INTRODUCTION

The selective catalytic reduction (SCR) is widely used for the removal of nitrogen oxides (NO_x) in exhaust-gas aftertreatment systems of vehicles with diesel engines.^{1–4} In the presence of suitable heterogeneous catalysts, NO_x can be reduced by reaction with ammonia injected into the exhaust-gas flow. Transition-metal zeolite catalysts are available for SCR and are predominately used in automotive applications.^{2,4–6} The most widely used zeolite catalysts are the iron-based Fe-ZSM-5^{7–9} and copper-exchanged zeolites with the chabazite structure, particularly Cu-SSZ-13 and Cu-SAPO-34.^{10,11} The latter are particularly attractive due to their hydrothermal stability. More recently, the chabazite iron-catalyst Fe-SSZ-13 has also been demonstrated to show high-temperature SCR activity.¹²

Both the structure of the catalytically active metal centers in these catalysts and the catalytic mechanism of the SCR reaction have been studied extensively both experimentally and computationally. For the chabazite-based catalysts, the nature of the catalytically active sites has been investigated, both for Cu-SSZ-13^{13–16} and Cu-SAPO-34¹⁷ as well as for Fe-SSZ-13.^{18,19} Different studies agree that the major active species are single Cu^{II} or Fe^{III} centers located in the 6-membered or 8-membered rings of the zeolite framework, where they balance the negative charge of an Al³⁺ site. Depending on the coordination of further ligands such as water, NH₃, or NO as well as on temperature, the Cu centers can detach from the zeolite framework and can become mobile.^{15,20–24} On the other hand, Fe centers are believed to be more strongly bound and remain immobile within the zeolite framework.¹⁹

Even though many details of the catalytic mechanism have been elucidated, the SCR mechanism is still not fully understood.^{25–28} This is particularly true for Fe-exchanged zeolite catalysts, which have been studied less extensively than Cu-exchanged zeolite catalysts. Although for Cu catalysts computational studies explored different possible mechanistic

pathways,^{17,22,29–32} a comprehensive computational picture of the SCR mechanism for Fe catalysts is still lacking.^{26,33} Here, we aim at closing this gap by computationally exploring different possible mechanistic pathways for the reduction half-cycle of the SCR reaction with Fe catalysts. In addition, we set out to compare these reaction pathways for Fe and Cu zeolite catalysts to provide a unified picture.

There is general agreement that the SCR reaction proceeds via the redox cycle schematically shown in Figure 1a (ref 28). First, in the reduction half-cycle, NO and NH₃ react to N₂ and H₂O while reducing the catalytic metal center. Second, in the oxidation half-cycle, the catalytic metal center is reoxidized. This slow reoxidation is generally considered to be the rate-determining step. The reaction equation of the oxidation half-cycle will differ depending on the availability of NO₂ (see Figure 1a). Different detailed mechanistic proposals have been made for the oxidation half-cycle with Cu-exchanged zeolite catalysts under both standard SCR and fast SCR conditions.^{17,22,29–31,34} Most likely, the oxidation half-cycle proceeds via the formation of dimeric Cu species.^{22,35}

Here, we focus on the reduction half-cycle of the SCR reaction. Most generally, this first part of the SCR reaction can proceed via two different mechanistic pathways (see Figure 1b) by adsorbing either NH₃ or NO at the catalytic metal center in the first step. If NH₃ is coordinated first (NH₃-first pathway), a proton needs to be transferred either to another ligand or to the zeolite framework. NO can subsequently either be adsorbed at the metal center or directly attack the coordinated NH₂ ligand. Both possibilities lead to the release of N₂ and H₂O via an NH₂NO intermediate. If NO reacts first (NO-first pathway), one generally assumes the intermediate formation of a HONO ligand, either via an intermediate NO

Received: March 4, 2019

Accepted: April 2, 2019

Published: May 1, 2019

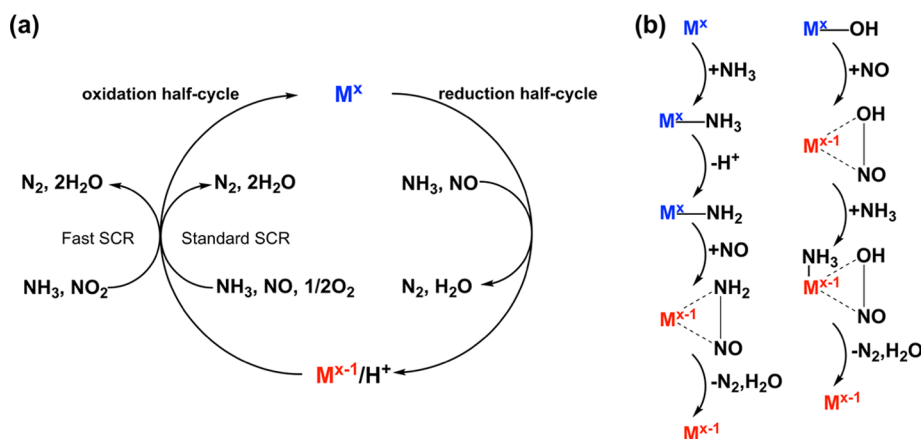


Figure 1. (a) Schematic redox cycle for the standard and the fast SCR reaction. M^x (blue) denotes the oxidized catalytic metal center, whereas M^{x-1} (red) refers to a reduced form of the catalytic metal center. (b) Possible simplified reaction mechanisms for the SCR reduction half-cycle on the NH_3 -first pathway (left) and the NO -first pathway (right).

complex or via a direct attack of NO at an OH^- ligand. Subsequently, this HONO ligand reacts with NH_3 to form N_2 and $2\text{H}_2\text{O}$. Again, this step could proceed either via intermediates in which NH_3 is coordinated with the metal center or via a direct attack of NH_3 at the HONO ligand.

Previous computational studies for Cu-exchanged zeolite catalysts provide an ambiguous picture for the reduction half-cycle. Although refs 17, 22, 30 assume the SCR reduction half-cycle to proceed via the NH_3 -first pathway, refs 29, 31 consider the NO -first pathway. In ref 34, both pathways are explored, with the computational results suggesting that the reaction via a HONO intermediate is preferred. Further details of these different mechanistic proposals will be discussed below. Based on kinetic and spectroscopic studies of SCR catalyzed by Fe-ZSM-5, mechanisms proceeding via different variants of an NO -first pathway have been suggested,^{36,37} whereas computational investigations assumed mechanisms via the NH_3 -first pathway.^{33,38}

2. RESULTS AND DISCUSSION

To computationally explore the mechanism of the SCR reaction with Fe and Cu zeolite catalysts, we employ minimal models of the active center^{33,39} as shown in Figure 2b,c. These models are based on the optimized structure of the model shown in Figure 2a. In both cases, we consider overall neutral models of the active center (see the Supporting Information for further discussions). The use of a minimal active-site model will allow us to identify feasible reaction pathways and to reveal intrinsic mechanistic differences between Fe and Cu catalysts that are independent of the precise nature of the active center. A comparison to a larger active-site model as well as to an NH_3 -solvated active-site model is provided in the Supporting Information.

We start by considering possible reaction pathways for the reduction half-cycle of the SCR reaction with Fe-exchanged zeolite catalysts (see Figure 3) and start from the overall neutral model $[\text{Z}-\text{Fe}^{\text{III}}(\text{OH})_2]$ (A, see Figure 2b) with a d^5 high-spin electron configuration. Such species have been identified as the major monomeric Fe species in Fe-SSZ-13 catalysts.¹⁸

The first possible SCR reaction pathway (NH_3 -first pathway, see the right part of Figure 3a) starts with the adsorption of NH_3 , leading to $[\text{Z}-\text{Fe}^{\text{III}}(\text{OH})_2(\text{NH}_3)]$ (B). This step is

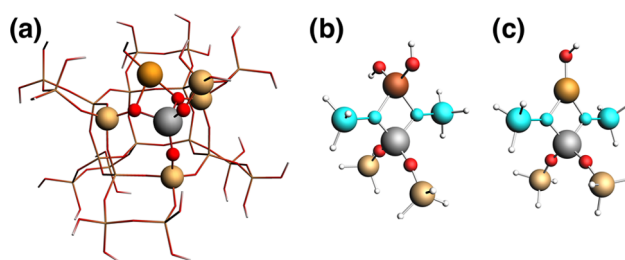


Figure 2. (a) Optimized molecular structure of a model of the active metal center in Cu-SSZ-13. The atoms shown herein as balls and sticks are used in the minimal model of the catalytic centers employed in our calculations. (b) Optimized molecular structure of our starting model of the active centers in Fe-doped zeolite catalysts $[\text{Z}-\text{Fe}^{\text{III}}(\text{OH})_2]$. (c) Optimized molecular structure of our starting model of the active centers in Cu-doped zeolite catalysts $[\text{Z}-\text{Cu}^{\text{II}}(\text{OH})]$. Color code: Fe (dark brown), Cu (orange), O (red), N (blue), Al (gray), Si (light brown), and H (white). The coordinates of the atoms highlighted in cyan for models (b) and (c) are kept fixed at their positions in model (a) in all our calculations.

exothermic by -56 kJ/mol. Subsequently, a proton is shifted from the NH_3 ligand to one of the OH^- ligands, resulting in $[\text{Z}-\text{Fe}^{\text{III}}(\text{OH})(\text{H}_2\text{O})(\text{NH}_3)]$ (C), which can abstract a water molecule to arrive at $[\text{Z}-\text{Fe}^{\text{III}}(\text{OH})(\text{NH}_2)]$ (D). This proton shift and the water abstraction are endothermic and altogether require 82 kJ/mol. However, we could not identify any feasible alternatives on the NH_3 -first pathway.

Intermediate D can now react with NO in two different ways. First, NO can be coordinated to form $[\text{Z}-\text{Fe}^{\text{II}}(\text{OH})(\text{NH}_2)(\text{NO})]$ (E), reducing Fe^{III} to low-spin ($S = 0$) Fe^{II} . A rearrangement, in which the NH_2 ligand shifts to form a $\text{N}-\text{N}$ bond, then leads to $[\text{Z}-\text{Fe}^{\text{II}}(\text{OH})(\text{NONH}_2)]$ (G). According to our computations, G has a high-spin ($S = 2$) ground state, i.e., this step requires a spin crossover. Species G can release N_2 and H_2O via (I), finally resulting in a reduced iron species $[\text{Z}-\text{Fe}^{\text{II}}(\text{OH})]$ (J). Alternatively, one could assume a direct reaction of NO from the gas phase with the NH_2 ligand. The only plausible resulting intermediate that we could find in our calculations is species F, which contains an $\text{ON}-\text{NH}_2$ ligand coordinated with the Fe center via the nitrogen atoms. Again, our computations show a high-spin ($S = 2$) ground state for this species, which could further react to J under release of N_2 and H_2O . However, the formation of the alternative

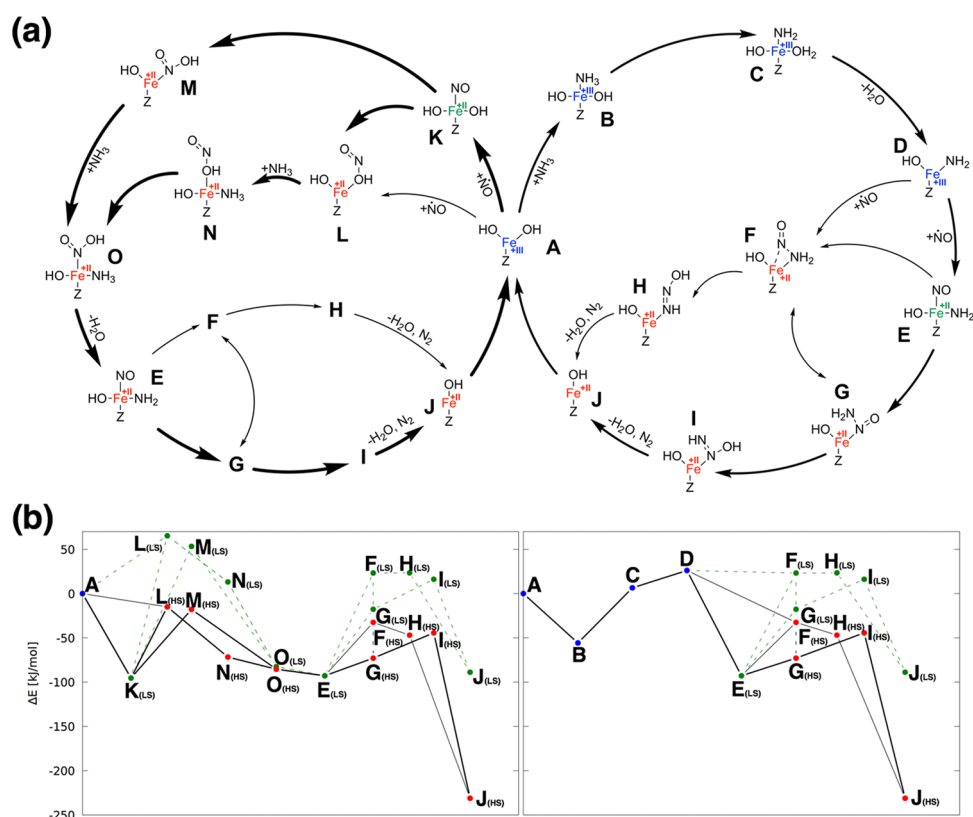


Figure 3. (a) Reaction pathways considered for the mechanism of the reduction half-cycle of the SCR reaction catalyzed by Fe-exchanged zeolite catalysts. Both pathways starting with the adsorption of NO (left) and with the adsorption of NH_3 (right) are considered. (b) Calculated energy profiles (BP86/TZ2P) for the considered reaction pathways. For all Fe^{III} species (blue), the high-spin ($S = 5/2$) state is the ground state. For the Fe^{II} species, the calculated energies of both the high-spin ($S = 2$, red) and low-spin ($S = 0$, green) states are included.

intermediate **E** from **D** is exothermic by -119 kJ/mol, whereas **F** is 60 kJ/mol higher in energy than **E**. Therefore, this reaction path would most likely proceed via **E** with a coordination of NO with the iron center instead of a direct reaction of NO from the gas phase.

The second possible SCR reaction pathway (NO-first pathway, see the left part of Figure 3a) starts with the adsorption of NO, leading to $[\text{Z}-\text{Fe}^{\text{II}}(\text{OH})_2(\text{NO})]$ (**K**) while reducing the Fe center to low-spin ($S = 0$) Fe^{II} . This step is exothermic by -95 kJ/mol. The subsequent formation of an intermediate $[\text{Z}-\text{Fe}^{\text{II}}(\text{OH})_2(\text{NO})(\text{NH}_3)]$, in which NO and NH_3 are simultaneously coordinated with the Fe center, was not stable in our computations. Instead, **K** rearranges under formation of a HONO ligand, which could be coordinated either via an oxygen atom (**L**) or via the nitrogen atom (**M**), which are almost equal in energy. Both **L** and **M** have a high-spin ($S = 2$) ground state in our calculations, and the formation of the HONO ligand thus requires a spin crossover.

After the formation of **L** or **M**, NH_3 can coordinate, resulting in $[\text{Z}-\text{Fe}^{\text{II}}(\text{HONO})(\text{NH}_3)]$, with HONO coordinated via the oxygen atom (**N**) or via the nitrogen atom (**O**), respectively. This step is exothermic by 57 and 68 kJ/mol, respectively, and the two intermediates **N** and **O** differ in energy by only 14 kJ/mol. Abstraction of H_2O from **O** leads to $[\text{Z}-\text{Fe}^{\text{II}}(\text{OH})(\text{NH}_2)(\text{NO})]$ (**E**), which can release N_2 and H_2O via **G** and **I** or via **F** and **I** (see above).

Overall, according to our calculations, a mechanism via the NO-first pathway seems more likely as it does not require the energetically unfavorable intermediate **D** that needs to be formed on the NH_3 -first pathway. The highest-energy

intermediates on the NO-first pathway are **L** and **M**, which are 41–44 kJ/mol lower in energy than **D**. Both the mechanisms via **L** and **M**, i.e., via the formation of a HONO ligand and subsequent adsorption of NH_3 , are possible according to our computational results. According to our calculations, all accessible reaction pathways require a spin crossover from low-spin to high-spin Fe^{II} . However, because of the known insufficiencies of density-functional approximations for spin-state energy differences,^{40–42} it cannot be ruled out that for some of our high-spin Fe^{II} intermediates the corresponding low-spin species are actually more stable (see the Supporting Information for additional calculations and discussion).

For comparison, we considered the same possible reaction pathways for the SCR reaction catalyzed by Cu-exchanged zeolites (see Figure 4). Here, we start from the overall neutral model $[\text{Z}-\text{Cu}^{\text{II}}(\text{OH})]$ (**A**, see Figure 2c), which is in line with the neutral models considered in refs 22, 29, 34. Similar results are obtained for a negatively charged model $[\text{Z}-\text{Cu}^{\text{II}}(\text{OH})_2]^-$ resembling the models used in refs 17, 30, 31 (see the Supporting Information).

For the NH_3 -first pathway (see the right part of Figure 4), the same possible reaction steps and intermediates as for the case of Fe-exchanged zeolite catalysts were found, even though the relative energies of the different intermediates differ. Most importantly, the transfer of a proton from the NH_3 ligand to the OH ligand and the subsequent abstraction of water (**B** to **D**) now require only 56 kJ/mol, with **D** lying lower in energy by 20 kJ/mol than the starting point **A**. Note that some previous calculations assume a proton transfer to the zeolite

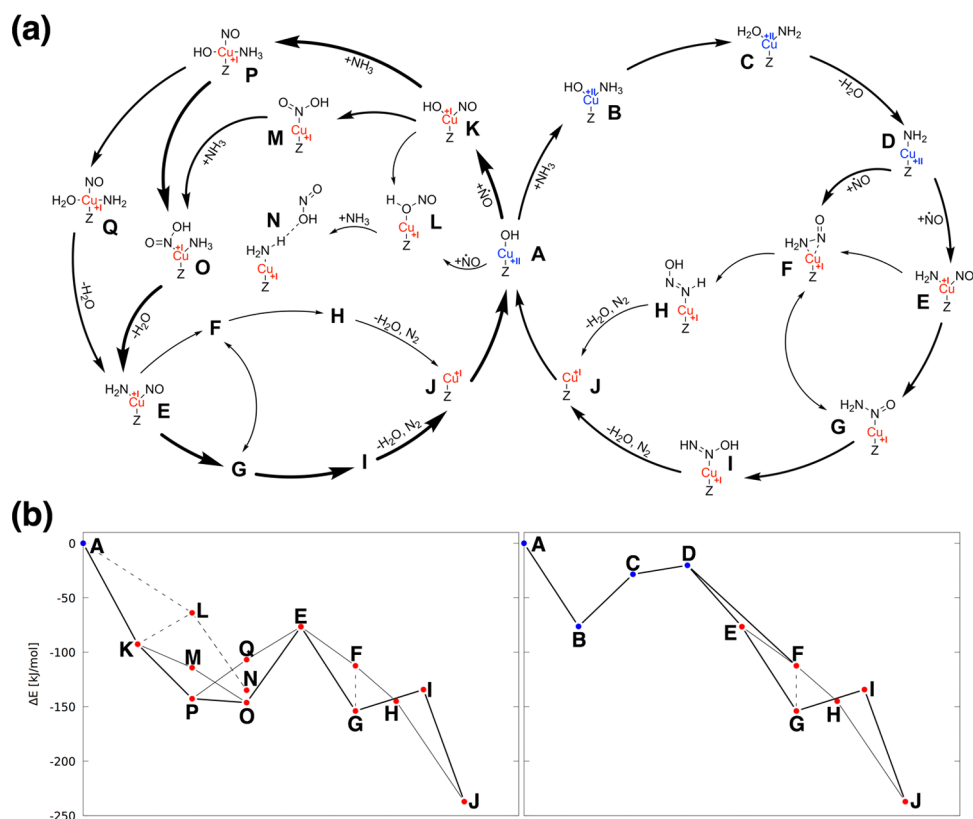


Figure 4. (a) Reaction pathways considered for the mechanism of the reduction half-cycle of the SCR reaction catalyzed by Cu-exchanged zeolite catalysts. Both pathways starting with the adsorption of NO (left) and with the adsorption of NH₃ (right) are considered. (b) Calculated energy profiles (BP86/TZ2P) for the considered reaction pathways.

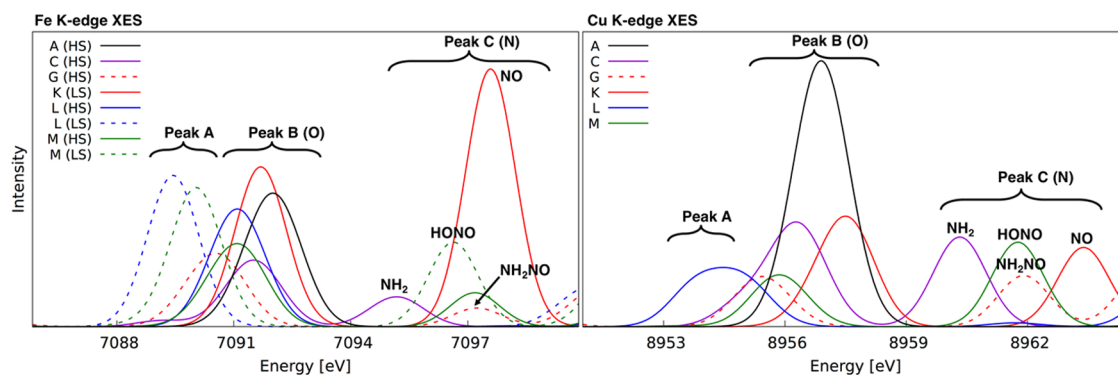


Figure 5. Calculated (BP86/QZ4P) Fe K-edge and Cu K-edge XES spectra of selected intermediates on the considered catalytic reaction pathways of the SCR reaction with Fe catalysts (left) and with Cu catalysts (right). The indicated assignment refers to the in operando measurements of refs 45 and 32. Calculated XES spectra of all considered intermediates are shown in the Supporting Information.

framework in this step,^{17,22,30} which cannot be described by our small model. However, according to ref 17, such a proton transfer would require 114 kJ/mol. The further reactions via the formation and decomposition of an ON–NH₂ ligand (F or G) can proceed via steps that are all exothermic or require only little energy.

For the NO-first pathway (see the left part of Figure 4), there are some fundamental differences to the case of Fe-exchanged zeolite catalysts. After coordination of NO (K), the formation of a HONO ligand coordinated via its oxygen atom L leads to the dissociation of the HONO ligand after coordination of NH₃ (N). Thus, this path does not lead to the reduction of NO. Instead, the formation of a HONO ligand coordinated via its nitrogen (M) atom is preferred and

leads to O after coordination of NH₃. Alternatively, ammonia can coordinate with K under formation of P. Such an intermediate was not available in the case of an Fe zeolite catalyst. Here, the formation of P is energetically preferred compared to that of M by 28 kJ/mol, but both can further react to the same intermediate O. The remaining steps proceed via the formation of E, which is endothermic by +70 kJ/mol, and match those discussed above for the Fe zeolite catalyst.

Overall, also for Cu-based zeolite catalysts, the NO-first pathway seems to be preferred, even though on the NH₃-first pathway the high-energy intermediate D is more favorable in the case of a Cu catalyst than for an Fe catalyst. However, for a Cu catalyst, the NO-first pathway cannot proceed via an intermediate L as it does for Fe catalysts. Instead, the SCR

reaction will most likely proceed via intermediate **P**, which is not accessible with an Fe catalyst. The only slightly disfavored route via **M** is available for both Cu and Fe catalysts.

Our computational elucidation of the possible catalytic reaction pathways provides the basis for spectroscopic identification of catalytic intermediates. A unique method for this purpose is provided by X-ray spectroscopy.^{43,44} Based on in operando valence-to-core X-ray emission spectroscopy (VtC-XES), we previously observed a peak at ca. 7087 eV (“peak A”) for Fe-ZSM-5 that appears at lower energies than the peak due to the lone pair at ligands coordinated via oxygen (ca. 7091 eV, “peak B”) and the peak due to the lone pair at ligands coordinated via nitrogen (ca. 7096 eV, “peak C”). This led us to the conclusion that with Fe-ZSM-5 the SCR reaction proceeds via the NO-first pathway⁴⁵ with an intermediate featuring HONO coordinated via its central oxygen atom that bears a positive partial charge. On the other hand, for Cu-SSZ-13, such a peak is absent from the in operando XES spectra and thus a different mechanism via the NH₃-first pathway seems to be employed.³²

To reconcile these earlier spectroscopic results with our present computational study, we calculated the XES spectra of all considered intermediates. The calculated spectra of selected intermediates are shown in Figure 5 (see the Supporting Information for all calculated spectra). These results confirm the previous assignment of peaks B and C. For Fe catalysts, a spectroscopic feature that is clearly shifted to lower energies by ca. 3 eV with respect to peak B is found only for the low-spin states of **L**, **N**, and **M**. Thus, the peak A that was experimentally observed in ref 45 could indeed indicate that the SCR reaction proceeds via the NO-first pathway for Fe catalysts. However, this assignment holds only if the reaction proceeds via low-spin Fe^{II} intermediates that are not the ground state in our calculations. On the other hand, we can clearly rule out that peak A is due to the coordination of NO with the iron center, as was suggested in ref 28.

Of the intermediates considered for Cu catalysts, only the intermediates **L** and **N** show a peak clearly shifted to lower energies compared to peak B in the calculated spectra. However, these species do not lie on a feasible reaction path that leads to the reduction of NO. Thus, the absence of such a peak in the in operando XES spectra reported in ref 32 does not allow us to distinguish between the NH₃-first and NO-first (via **M** or **P**) reaction pathways.

3. CONCLUSIONS

We could computationally identify several possible catalytic reaction pathways for the reduction half-cycle of the selective catalytic reduction of NO_x with Fe- and Cu-exchanged zeolite catalysts. They provide a comprehensive picture that unifies several previous mechanistic proposals. We find that both for Fe and for Cu catalysts different reaction pathways are available and both an NH₃-first pathway and an NO-first pathway seem feasible, of which the NO-first pathway is preferred according to our computational results. Although on both pathways a coordination of NO at the metal center and its direct reaction of NO with ligands coordinated at the metal center are both possible, NH₃ can react further only after its adsorption at the metal center. However, some of the available reaction pathways differ for Fe and Cu catalysts. Although for Fe catalysts the SCR reaction can proceed via an intermediate with a HONO ligand coordinated with the metal center via its central oxygen atoms, this pathway is not possible for Cu

catalysts. This is in agreement with previous in operando XES measurements. On the other hand, for Cu catalysts, a reaction path via an intermediate that simultaneously coordinates NO and NH₃ is available, which is inaccessible for Fe catalysts.

A distinction between the different pathways that are feasible according to the present computational results will require further spectroscopic and computational studies. Computationally, larger models of the active site as well as the use of higher accuracy computational methods could decrease the computational error bars and possibly distinguish between different pathways. For Fe catalysts, quantum-chemical methods beyond density-functional theory (DFT) might be required to provide more accurate spin-state energy differences. Moreover, the determination of the transition states connecting different intermediates as well as the calculation of the corresponding activation energies will be required for a complete picture. Of course, additional reaction pathways might become possible when considering larger active-site models, e.g., by involving a second metal center or by allowing for mobile, NH₃-solvated metal centers. Nevertheless, the unified mechanistic picture provided here will form an ideal starting point for such future studies.

4. COMPUTATIONAL METHODS

The molecular structures of all considered models have been optimized using DFT as implemented in the Amsterdam density functional program package,^{46,47} employing the BP86 generalized-gradient approximation exchange–correlation functional^{48,49} in combination with the Slater-type TZ2P basis set.⁵⁰ Further details on the construction of our model structures are given in the Supporting Information. All relative energies refer to the differences in the total electronic energy without additional corrections. For all Fe^{III} species, the ground state is the high-spin ($S = 5/2$) state, whereas for Fe^{II}, both the low-spin ($S = 0$) and the high-spin ($S = 2$) states were considered. For all Cu^I models, we assumed a closed-shell singlet ground state, whereas for all Cu^{II} models, spin-unrestricted calculations were performed for the doublet ($S = 1/2$) ground state. Optimized molecular structures as well as all calculated relative energies are included in the Supporting Information. For comparison, all calculations have been repeated using the B3LYP hybrid exchange–correlation functional⁵¹ with the same basis set as well as including Grimme’s D3 dispersion correction⁵² (see the Supporting Information). XES spectra were recorded using the standard Δ DFT approach^{53,54} including higher-order intensity contributions⁵⁵ with BP86/QZ4P. Fe K-edge and Cu K-edge spectra have been shifted by 181.34 eV and by 229.14 eV, respectively, to align them with the experimental energy scale.

■ ASSOCIATED CONTENT

Supporting Information

The Supporting Information is available free of charge on the ACS Publications website at DOI: 10.1021/acsomega.9b00600.

Construction of the active-site model; additional computational results (comparison of exchange–correlation functionals, assessment of dispersion correction, and validation of the active-site model), structures and relative energies of all considered species (PDF)

xyz-files of optimized structures of all considered species (ZIP)

AUTHOR INFORMATION

Corresponding Author

*E-mail: c.jacob@tu-braunschweig.de.

ORCID

Christoph R. Jacob: 0000-0002-6227-8476

Notes

The authors declare no competing financial interest.

ACKNOWLEDGMENTS

We acknowledge support by the Deutsche Forschungsgemeinschaft (DFG) via the Open Access Publication Funds of the Technische Universität Braunschweig.

REFERENCES

- (1) Busca, G.; Lietti, L.; Ramis, G.; Berti, F. Chemical and mechanistic aspects of the selective catalytic reduction of NO_x by ammonia over oxide catalysts: A review. *Appl. Catal., B* **1998**, *18*, 1–36.
- (2) Koebel, M.; Elsener, M.; Kleemann, M. Urea-SCR: a promising technique to reduce NO_x emissions from automotive diesel engines. *Catal. Today* **2000**, *59*, 335–345.
- (3) Brandenberger, S.; Kröcher, O.; Tisser, A.; Althoff, R. The State of the Art in Selective Catalytic Reduction of NO_x by Ammonia Using Metal-Exchanged Zeolite Catalysts. *Catal. Rev.* **2008**, *50*, 492–531.
- (4) Guan, B.; Zhan, R.; Lin, H.; Huang, Z. Review of state of the art technologies of selective catalytic reduction of NO_x from diesel engine exhaust. *Appl. Therm. Eng.* **2014**, *66*, 395–414.
- (5) Beale, A. M.; Gao, F.; Lezcano-Gonzalez, I.; Peden, C. H. F.; Szanyi, J. Recent advances in automotive catalysis for NO_x emission control by small-pore microporous materials. *Chem. Soc. Rev.* **2015**, *44*, 7371–7405.
- (6) Xin, Y.; Li, Q.; Zhang, Z. Zeolitic Materials for DeNO_x Selective Catalytic Reduction. *ChemCatChem* **2018**, *10*, 29–41.
- (7) Long, R. Q.; Yang, R. T. Catalytic Performance of Fe–ZSM-5 Catalysts for Selective Catalytic Reduction of Nitric Oxide by Ammonia. *J. Catal.* **1999**, *188*, 332–339.
- (8) Schwidder, M.; Kumar, M. S.; Klementiev, K.; Pohl, M. M.; Brückner, A.; Grünert, W. Selective reduction of NO with Fe-ZSM-5 catalysts of low Fe content: I. Relations between active site structure and catalytic performance. *J. Catal.* **2005**, *231*, 314–330.
- (9) Grossale, A.; Nova, I.; Tronconi, E. Study of a Fe–zeolite-based system as NH₃-SCR catalyst for diesel exhaust after treatment. *Catal. Today* **2008**, *136*, 18–27.
- (10) Schmieg, S. J.; Oh, S. H.; Kim, C. H.; Brown, D. B.; Lee, J. H.; Peden, C. H. F.; Kim, D. H. Thermal durability of Cu-CHA NH₃-SCR catalysts for diesel NO_x reduction. *Catal. Today* **2012**, *184*, 252–261.
- (11) Blakeman, P. G.; Burkholder, E. M.; Chen, H.-Y.; Collier, J. E.; Fedeyko, J. M.; Jobson, H.; Rajaram, R. R. The role of pore size on the thermal stability of zeolite supported Cu SCR catalysts. *Catal. Today* **2014**, *231*, 56–63.
- (12) Gao, F.; Kollár, M.; Kukkadapu, R. K.; Washton, N. M.; Wang, Y.; Szanyi, J.; Peden, C. H. F. Fe/SSZ-13 as an NH₃-SCR catalyst: A reaction kinetics and FTIR/Mössbauer spectroscopic study. *Appl. Catal., B* **2015**, *164*, 407–419.
- (13) Gao, F.; Walter, E. D.; Karp, E. M.; Luo, J.; Tonkyn, R. G.; Kwak, J. H.; Szanyi, J.; Peden, C. H. F. Structure-activity relationships in NH₃-SCR over Cu-SSZ-13 as probed by reaction kinetics and EPR studies. *J. Catal.* **2013**, *300*, 20–29.
- (14) Bates, S. A.; Verma, A. A.; Paolucci, C.; Parekh, A. A.; Anggara, T.; Yezerets, A.; Schneider, W. F.; Miller, J. T.; Delgass, W. N.; Ribeiro, F. H. Identification of the active Cu site in standard selective catalytic reduction with ammonia on Cu-SSZ-13. *J. Catal.* **2014**, *312*, 87–97.
- (15) Moreno-González, M.; Hueso, B.; Boronat, M.; Blasco, T.; Corma, A. Ammonia-Containing Species Formed in Cu-Chabazite As Per In Situ EPR, Solid-State NMR, and DFT Calculations. *J. Phys. Chem. Lett.* **2015**, 1011–1017.
- (16) Borfecchia, E.; Lomachenko, K. A.; Giordanino, F.; Falsig, H.; Beato, P.; Soldatov, A. V.; Bordiga, S.; Lamberti, C. Revisiting the nature of Cu sites in the activated Cu-SSZ-13 catalyst for SCR reaction. *Chem. Sci.* **2015**, *6*, 548–563.
- (17) Li, Y.; Deng, J.; Song, W.; Liu, J.; Zhao, Z.; Gao, M.; Wei, Y.; Zhao, L. Nature of Cu Species in Cu-SAPO-18 Catalyst for NH₃-SCR: Combination of Experiments and DFT Calculations. *J. Phys. Chem. C* **2016**, *120*, 14669–14680.
- (18) Gao, F.; Zheng, Y.; Kukkadapu, R. K.; Wang, Y.; Walter, E. D.; Schwenzer, B.; Szanyi, J.; Peden, C. H. F. Iron Loading Effects in Fe/SSZ-13 NH₃-SCR Catalysts: Nature of the Fe Ions and Structure-Function Relationships. *ACS Catal.* **2016**, *6*, 2939–2954.
- (19) Zhang, R.; Anderst, E.; Groden, K.; McEwen, J.-S. Modeling the Adsorption of NO and NH₃ on Fe-SSZ-13 from First-Principles: A DFT Study. *Ind. Eng. Chem. Res.* **2018**, *57*, 13396–13405.
- (20) Zhang, R.; McEwen, J.-S.; Kollár, M.; Gao, F.; Wang, Y.; Szanyi, J.; Peden, C. H. F. NO Chemisorption on Cu/SSZ-13: A Comparative Study from Infrared Spectroscopy and DFT Calculations. *ACS Catal.* **2014**, *4*, 4093–4105.
- (21) Zhang, R.; Li, H.; McEwen, J.-S. Chemical Sensitivity of Valence-to-Core X-ray Emission Spectroscopy Due to the Ligand and the Oxidation State: A Computational Study on Cu-SSZ-13 with Multiple H₂O and NH₃ Adsorption. *J. Phys. Chem. C* **2017**, *121*, 25759–25767.
- (22) Paolucci, C.; Parekh, A. A.; Khurana, I.; Di Iorio, J. R.; Li, H.; Albarracín Caballero, J. D.; Shih, A. J.; Anggara, T.; Delgass, W. N.; Miller, J. T.; Ribeiro, F. H.; Gounder, R.; Schneider, W. F. Catalysis in a Cage: Condition-Dependent Speciation and Dynamics of Exchanged Cu Cations in SSZ-13 Zeolites. *J. Am. Chem. Soc.* **2016**, *138*, 6028–6048.
- (23) Kerkeni, B.; Berthout, D.; Berthomieu, D.; Doronkin, D. E.; Casapu, M.; Grunwaldt, J. D.; Chizallet, C. Copper Coordination to Water and Ammonia in CuII-Exchanged SSZ-13: Atomistic Insights from DFT Calculations and in Situ XAS Experiments. *J. Phys. Chem. C* **2018**, *122*, 16741–16755.
- (24) Chen, P.; Khetan, A.; Jabłońska, M.; Simböck, J.; Muhler, M.; Palkovits, R.; Pitsch, H.; Simon, U. Local dynamics of copper active sites in zeolite catalysts for selective catalytic reduction of NO_x with NH₃. *Appl. Catal., B* **2018**, *237*, 263–272.
- (25) Gao, F.; Kwak, J. H.; Szanyi, J.; Peden, C. H. F. Current Understanding of Cu-Exchanged Chabazite Molecular Sieves for Use as Commercial Diesel Engine DeNO_x Catalysts. *Top. Catal.* **2013**, *56*, 1441–1459.
- (26) Mao, Y.; Wang, H.-F.; Hu, P. Theoretical investigation of NH₃-SCR processes over zeolites: A review. *Int. J. Quantum Chem.* **2015**, *115*, 618–630.
- (27) Paolucci, C.; di Iorio, J. R.; Ribeiro, F. H.; Gounder, R.; Schneider, W. F. *Advances in Catalysis*; Song, C., Ed.; Academic Press, 2016; Vol. 59, pp 1–107.
- (28) Jiang, T.; Lobo, R. F. *Structure and Bonding*; SpringerLink, Springer: Berlin, 2018; pp 1–24.
- (29) Janssens, T. V. W.; Falsig, H.; Lundegaard, L. F.; Vennestrøm, P. N. R.; Rasmussen, S. B.; Moses, P. G.; Giordanino, F.; Borfecchia, E.; Lomachenko, K. A.; Lamberti, C.; Bordiga, S.; Godiksen, A.; Mossin, S.; Beato, P. A Consistent Reaction Scheme for the Selective Catalytic Reduction of Nitrogen Oxides with Ammonia. *ACS Catal.* **2015**, *5*, 2832–2845.
- (30) Paolucci, C.; Verma, A. A.; Bates, S. A.; Kispersky, V. F.; Miller, J. T.; Gounder, R.; Delgass, W. N.; Ribeiro, F. H.; Schneider, W. F. Isolation of the Copper Redox Steps in the Standard Selective Catalytic Reduction on Cu-SSZ-13. *Angew. Chem., Int. Ed.* **2014**, *53*, 11828–11833.
- (31) Mao, Y.; Wang, Z.; Wang, H.-F.; Hu, P. Understanding Catalytic Reactions over Zeolites: A Density Functional Theory Study of Selective Catalytic Reduction of NO_x by NH₃ over Cu-SAPO-34. *ACS Catal.* **2016**, *6*, 7882–7891.

- (32) Günter, T.; Carvalho, H. W. P.; Doronkin, D. E.; Sheppard, T.; Glatzel, P.; Atkins, A. J.; Rudolph, J.; Jacob, C. R.; Casapu, M.; Grunwaldt, J.-D. Structural snapshots of the SCR reaction mechanism on Cu-SSZ-13. *Chem. Commun.* **2015**, *51*, 9227–9230.
- (33) Brüggemann, T. C.; Keil, F. J. Theoretical Investigation of the Mechanism of the Selective Catalytic Reduction of Nitrogen Oxide with Ammonia on Fe-Form Zeolites. *J. Phys. Chem. C* **2011**, *115*, 23854–23870.
- (34) Gao, F.; Mei, D.; Wang, Y.; Szanyi, J.; Peden, C. H. F. Selective Catalytic Reduction over Cu/SSZ-13: Linking Homo- and Heterogeneous Catalysis. *J. Am. Chem. Soc.* **2017**, *139*, 4935–4942.
- (35) Paolucci, C.; Khurana, I.; Parekh, A. A.; Li, S.; Shih, A. J.; Li, H.; Iorio, J. R. D.; Albarracin-Caballero, J. D.; Yezerets, A.; Miller, J. T.; Delgass, W. N.; Ribeiro, F. H.; Schneider, W. F.; Gounder, R. Dynamic multinuclear sites formed by mobilized copper ions in NO_x selective catalytic reduction. *Science* **2017**, *357*, 898–903.
- (36) Metkar, P. S.; Salazar, N.; Muncrief, R.; Balakotaiah, V.; Harold, M. P. Selective catalytic reduction of NO with NH₃ on iron zeolite monolithic catalysts: Steady-state and transient kinetics. *Appl. Catal., B* **2011**, *104*, 110–126.
- (37) Ruggeri, M. P.; Grossale, A.; Nova, I.; Tronconi, E.; Jirglova, H.; Sobalik, Z. FTIR in situ mechanistic study of the NH₃NO/NO₂ “Fast SCR” reaction over a commercial Fe-ZSM-5 catalyst. *Catal. Today* **2012**, *184*, 107–114.
- (38) Li, J.; Li, S. A DFT Study toward Understanding the High Activity of Fe-Exchanged Zeolites for the “Fast” Selective Catalytic Reduction of Nitrogen Oxides with Ammonia. *J. Phys. Chem. C* **2008**, *112*, 16938–16944.
- (39) Choi, S. H.; Wood, B. R.; Ryder, J. A.; Bell, A. T. X-ray Absorption Fine Structure Characterization of the Local Structure of Fe in Fe-ZSM-5. *J. Phys. Chem. B* **2003**, *107*, 11843–11851.
- (40) Reiher, M.; Salomon, O.; Hess, B. A. Reparameterization of hybrid functionals based on energy differences of states of different multiplicity. *Theor. Chem. Acc.* **2001**, *107*, 48–55.
- (41) Jacob, C. R.; Reiher, M. Spin in density-functional theory. *Int. J. Quantum Chem.* **2012**, *112*, 3661–3684.
- (42) Swart, M. Spin states of (bio)inorganic systems: Successes and pitfalls. *Int. J. Quantum Chem.* **2013**, *113*, 2–7.
- (43) Günter, T.; Doronkin, D. E.; Boubnov, A.; Carvalho, H. W. P.; Casapu, M.; Grunwaldt, J. D. The SCR of NO_x with NH₃ Examined by Novel X-ray Emission and X-ray Absorption Methods. *Top. Catal.* **2016**, *866*–874.
- (44) Lomachenko, K. A.; Borfecchia, E.; Bordiga, S.; Soldatov, A. V.; Beato, P.; Lamberti, C. Active sites in Cu-SSZ-13 deNO_x catalyst under reaction conditions: a XAS/XES perspective. *J. Phys.: Conf. Ser.* **2016**, *712*, No. 012041.
- (45) Boubnov, A.; Carvalho, H. W. P.; Doronkin, D. E.; Günter, T.; Gallo, E.; Atkins, A. J.; Jacob, C. R.; Grunwaldt, J.-D. Selective Catalytic Reduction of NO Over Fe-ZSM-5: Mechanistic Insights by Operando HERFD-XANES and Valence-to-Core X-ray Emission Spectroscopy. *J. Am. Chem. Soc.* **2014**, *136*, 13006–13015.
- (46) ADF, Amsterdam Density Functional Program; Theoretical Chemistry, Vrije Universiteit Amsterdam. <http://www.scm.com>.
- (47) te Velde, G.; Bickelhaupt, F. M.; Baerends, E. J.; Fonseca Guerra, C.; van Gisbergen, S. J. A.; Snijders, J. G.; Ziegler, T. Chemistry with ADF. *J. Comput. Chem.* **2001**, *22*, 931–967.
- (48) Becke, A. D. Density-functional exchange-energy approximation with correct asymptotic behavior. *Phys. Rev. A* **1988**, *38*, 3098–3100.
- (49) Perdew, J. P. Density-functional approximation for the correlation energy of the inhomogeneous electron gas. *Phys. Rev. B* **1986**, *33*, 8822–8824.
- (50) Van Lenthe, E.; Baerends, E. J. Optimized Slater-type basis sets for the elements 1–118. *J. Comput. Chem.* **2003**, *24*, 1142–1156.
- (51) Becke, A. D. Density-functional thermochemistry. III. The role of exact exchange. *J. Chem. Phys.* **1993**, *98*, 5648–5652.
- (52) Grimme, S.; Antony, J.; Ehrlich, S.; Krieg, H. A consistent and accurate ab initio parametrization of density functional dispersion correction (DFT-D) for the 94 elements H–Pu. *J. Chem. Phys.* **2010**, *132*, No. 154104.
- (53) Lee, N.; Petrenko, T.; Bergmann, U.; Neese, F.; DeBeer, S. Probing Valence Orbital Composition with Iron K β X-ray Emission Spectroscopy. *J. Am. Chem. Soc.* **2010**, *132*, 9715–9727.
- (54) Atkins, A. J.; Bauer, M.; Jacob, C. R. The chemical sensitivity of X-ray spectroscopy: high energy resolution XANES versus X-ray emission spectroscopy of substituted ferrocenes. *Phys. Chem. Chem. Phys.* **2013**, *15*, 8095–8105.
- (55) Bernadotte, S.; Atkins, A. J.; Jacob, C. R. Origin-independent calculation of quadrupole intensities in X-ray spectroscopy. *J. Chem. Phys.* **2012**, *137*, No. 204106.